PNAS Nexus, 2023, 2, 1–14
https://doi.org/10.1093/pnasnexus/pgad293
Advance access publication 31 October 2023
Research Report

# Closed-loop control of anesthetic state in nonhuman primates

Sourish Chakravarty[a,b,1], Jacob Donoghue[a,c,d,1], Ayan S. Waite[a,b], Meredith Mahnke[a], Indie C. Garwood[a,c,d], Sebastian Gallo[a], Earl K. Miller[a,d,2] and Emery N. Brown[a,b,c,d,e,f,*,2]

[a]The Picower Institute for Learning and Memory, Massachusetts Institute of Technology (MIT), Cambridge, MA 02139, USA
[b]Department of Anesthesia, Critical Care, and Pain Medicine, Massachusetts General Hospital, Boston, MA 02114, USA
[c]Harvard-MIT Division of Health Sciences and Technology, MIT, Cambridge, MA 02139, USA
[d]Department of Brain and Cognitive Sciences, MIT, Cambridge, MA 02139, USA
[e]Institute for Medical Engineering and Sciences, MIT, Cambridge, MA 02139, USA
[f]Department of Anaesthesia, Harvard Medical School, Boston, MA 02115, USA
*To whom correspondence should be addressed: Email: enb@neurostat.mit.edu
[1]S.C. and J.D. contributed equally to this work.
[2]E.K.M. and E.N.B. are co-senior authors.
**Edited By:** Dennis Discher

## Abstract

Research in human volunteers and surgical patients has shown that unconsciousness under general anesthesia can be reliably tracked using real-time electroencephalogram processing. Hence, a closed-loop anesthesia delivery (CLAD) system that maintains precisely specified levels of unconsciousness is feasible and would greatly aid intraoperative patient management. The US Federal Drug Administration has approved no CLAD system for human use due partly to a lack of testing in appropriate animal models. To address this key roadblock, we implement a nonhuman primate (NHP) CLAD system that controls the level of unconsciousness using the anesthetic propofol. The key system components are a local field potential (LFP) recording system; propofol pharmacokinetics and pharmacodynamic models; the control variable (LFP power between 20 and 30 Hz), a programmable infusion system and a linear quadratic integral controller. Our CLAD system accurately controlled the level of unconsciousness along two different 125-min dynamic target trajectories for 18 h and 45 min in nine experiments in two NHPs. System performance measures were comparable or superior to those in previous CLAD reports. We demonstrate that an NHP CLAD system can reliably and accurately control in real-time unconsciousness maintained by anesthesia. Our findings establish critical steps for CLAD systems' design and testing prior to human testing.

**Keywords:** closed-loop anesthesia delivery system, nonhuman primate, propofol

## Significance Statement

Unconsciousness, a fundamental component of general anesthesia, can be reliably tracked using real-time processing of a patient's brain waves recorded as electroencephalogram signals. A closed-loop anesthesia delivery (CLAD) system that precisely maintains unconsciousness would greatly aid intraoperative patient management. The Federal Drug Administration has approved no human CLAD system due partly to a lack of appropriate animal model studies. By combining neurophysiology, real-time signal processing, control theory with a programmable infusion pump system, we implemented a nonhuman primate (NHP) CLAD system that controls unconsciousness with the anesthetic propofol. Our CLAD system accurately and reliably controlled unconsciousness along different trajectories for nearly 19 h in nine experiments in two NHPs. Our findings establish critical steps for human testing of CLAD systems.

## Introduction

General anesthesia is a drug-induced reversible state consisting of antinociception, unconsciousness, amnesia, and immobility with maintenance of physiological stability (1, 2). Continuously monitoring a patient's physiological state during surgery and executing frequent management tasks to optimize care is fundamental to

**Competing Interest:** E.N.B holds patents on anesthetic state monitoring. E.N.B. holds founding interests in PASCALL, a start-up developing physiological monitoring systems; receives royalties from intellectual property through Massachusetts General Hospital licensed to Masimo. The interests of E.N.B. were reviewed and are managed by Massachusetts General Hospital and Mass General Brigham in accordance with their conflict-of-interest policies. S.C., J.D. and A.S.W. performed the research activity for this work, respectively, as a postdoctoral researcher, Ph.D. student and technical associate at MIT. S.C.'s current affiliation is with Alexion—AstraZeneca Rare Disease Unit, Boston, MA, USA, and also with MIT as a Research Affiliate. J.D. is currently the CEO and Co-Founder of Beacon Biosignals, Boston, MA, USA. A.S.W. is currently a graduate student at Brown University, Providence, RI, USA.
**Received:** March 26, 2023. **Revised:** August 13, 2023. **Accepted:** August 22, 2023

the practice of anesthesiology. During surgery, the American Society of Anesthesiologists practice standards require the presence throughout of a qualified anesthesia care provider and continual monitoring of oxygenation, ventilation, circulation, and temperature (3). The provider scans the relevant physiological variables (oxygen delivery, oxygen saturation, respiratory rate, expired carbon dioxide, heart rate, blood pressure, and temperature) every few minutes and takes actions to maintain stability. The time between actions can be longer if the provider becomes distracted with other management tasks. Automating repetitive task management, where possible, would mitigate fatigue, reduce human error and hence, benefit patient care.

An important task to automate is control of the patient's level of unconsciousness. Anesthetics create altered arousal states, such as unconsciousness, by producing oscillations in the brain's extracellular potentials that impede communication among regions (4–8). The brain states of patients are readily visible in the electroencephalogram (EEG). However, in the United States, anesthesia providers are not required to monitor a patient's brain state under general anesthesia. Most do not. To guard against awareness, in the absence of brain monitoring, anesthesiologists almost certainly administer anesthetic doses beyond what are needed to maintain an adequate level of unconsciousness. Postoperative cognitive disorders are common following anesthesia, particularly in the elderly (9–12). Among the contributory factors are anesthesia (general and regional), type of surgery, patient age, and patient state of health (13, 14). Recent studies suggest that use of brain monitoring to guide drug dosing can make general anesthesia less of a contributory factor (15). Level of unconsciousness under general anesthesia can be reliably tracked using real-time processing of EEG recordings (5, 6, 16–18). This suggests that the EEG can be used to develop a CLAD system to maintain precisely a specified level of unconsciousness.

Since the 1950s, EEG-based CLAD systems have been an active area of research (17, 19–26). CLAD systems have been studied in rodents (27–29), and outside the United States, in humans (20–26). The United States Food and Drug Administration (FDA) readily acknowledges the enormous benefits that CLAD systems, and more generally, physiological closed-loop control systems, can bring to patient care (30). However, this agency has approved no CLAD system for human testing in the United States. The FDA has identified testing of CLAD systems in appropriate animal models as a critical prerequisite for evaluating performance reliability and reproducibility prior to human testing (30). To address this critical gap, we develop and test a nonhuman primate (NHP) CLAD system for control of unconsciousness using the anesthetic propofol. We demonstrate that our propofol CLAD system can accurately and reliably maintain unconsciousness in simulation experiments and live experiments in two NHPs tracking dynamic target trajectories during nine experimental sessions.

# Results

## Overview of the propofol CLAD system

We use a linear quadratic integral (LQI) controller to implement a real-time CLAD system that continuously administers propofol to control unconsciousness in an NHP (Fig. 1). We chose the LQI control strategy because it offers a principled way to design optimal tracking algorithms, i.e. algorithms that have a high probability of accurately tracking a target (see section "Formulation of an NHP CLAD system"), and because it produces algorithms that

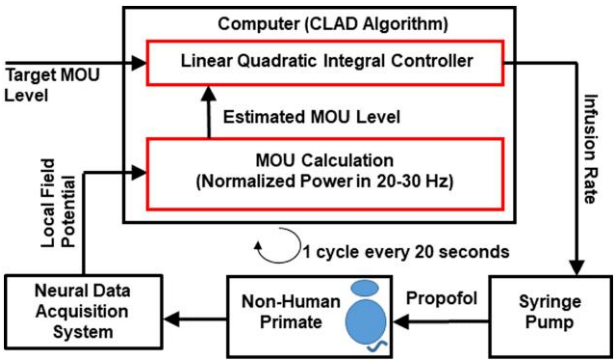


**Fig. 1.** Schematic of the propofol-based CLAD system for control of unconsciousness in an NHP. The user sets the target level of the marker of unconsciousness (MOU). The controller compares the difference between the target and estimated MOU. Based on that difference the controller changes the infusion rate of the syringe delivering propofol to the NHP. The neural data acquisition system records the LFP, computes an update of the MOU, which is the normalized power in the 20–30 Hz band and the control cycle begins again. The system duty cycle is 20 s.

are robust, i.e. that have low sensitivity to model errors and data disturbances (31). To start the control cycle, the user sets the target level of the marker of unconsciousness (MOU), a neurophysiological measure that tracks level of unconsciousness in real-time. The LQI controller computes the difference between the target and estimated MOUs. Based on that difference, the controller changes the infusion rate of the syringe pump delivering propofol intravenously to the NHP. The neural data acquisition system continuously records the local field potential (LFP). In each cycle, the MOU is computed from the LFP and the infusion rate is updated. The control cycle repeats every 20 s. The MOU, which is the normalized power in the 20–30 Hz band, is computed in real-time from the LFP recorded from a prefrontal cortical electrode by using multitaper spectral methods (6, 32, 33). The animal-specific parameters for the pharmacokinetic (PK) and pharmacodynamic (PD) models, and for the controller are estimated in a system identification experiment conducted prior to initiating control (see section "Materials and methods").

For safety purposes, because these types of experiments had not been previously attempted in NHPs, we initially restricted our protocols, PK and PD model development, MOU development, estimation algorithm and control algorithm studies to NHP-A. We also refrained from testing our CLAD work on a second animal until the pandemic was under better control. Once the experimental modeling and analyses paradigms were well developed in NPH-A and the pandemic was less of an issue, we tested the CLAD system in NHP-B. For this reason, we had more sessions with NHP-A than with NHP-B.

## Marker of unconsciousness: normalized 20–30 Hz power

To design the propofol CLAD system, we first establish an MOU to use as a control variable. Several EEG spectral features strongly correlate with unconsciousness in humans (6). In recent NHP experiments, Bastos et al. showed that cortical spike rates decrease (increase) with decreases (increases) in level of unconsciousness mediated by computer-controlled administration of propofol (7). We conducted 11 experimental sessions in two NHPs (10 for NHP-A and 1 for NHP-B) during which propofol was administered at predefined rates and LFP and neural spiking activity were recorded from prefrontal cortical electrodes. We looked to identify

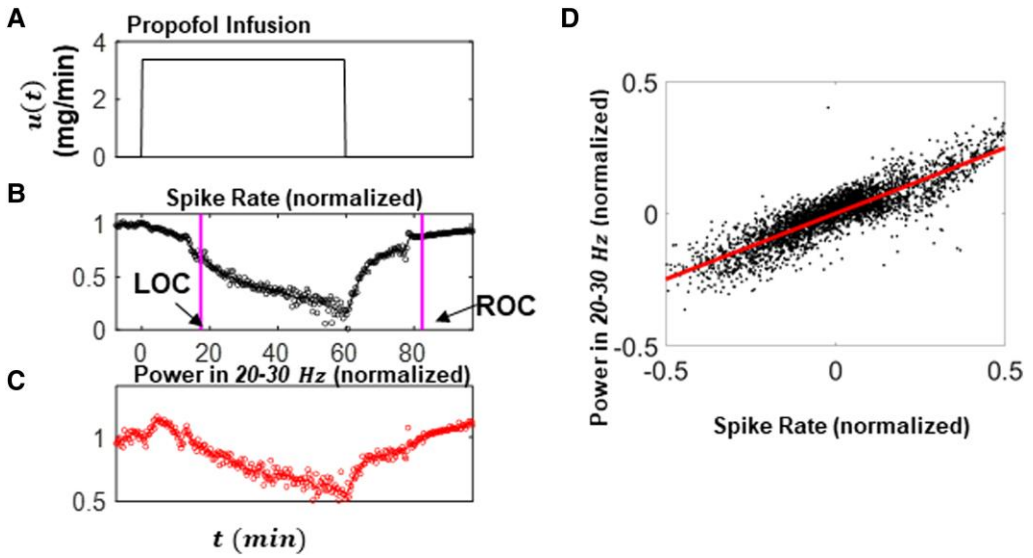


**Fig. 2.** A single experimental session for NHP-B showing the neurophysiological activity recorded from a single prefrontal cortex electrode in response to a constant propofol infusion (A–C). A) 60-min propofol infusion at 3.38 mg/min. B) Normalized spike rate. The first vertical magenta line is loss of consciousness (LOC) and the second vertical magenta line is recovery of consciousness (ROC). C) Normalized power in the 20–30 Hz band. D) Plot of normalized power in the 20–30 Hz band versus the normalized spike rates taken from 11 experimental sessions in NHP-A and NHP-B. The data from each recording session were centered about their session means. The correlation is 0.8823 [95% confidence interval: (0.8749, 0.8894)]. The solid red line is the linear regression fit. Corresponding plots for each of the 11 individual recording sessions are given in Figs. S1 and S2.

as an MOU an LFP spectral feature that tracked the changes in cortical spike rates associated with changes in the level of propofol-mediated unconsciousness.

To illustrate, propofol was administered to NHP-B at a constant infusion rate of 3.38 mg/min for 60 min (Fig. 2A). This rate was within the typical maintenance dose range of propofol-mediated unconsciousness in NHPs (34). Following Bastos et al., we identified loss of consciousness (LOC) as the time at which the animal's eyes closed and remained closed for at least 5 min (Fig. 2B, the first vertical magenta line) (7). Using their convention, we identified recovery of consciousness (ROC) as the time at which the animal opened its eyes for the first time after LOC [Fig. 2B, the second vertical magenta line (7)]. We defined the period of unconsciousness as the time between LOC and ROC (Fig. 2B). To identify possible markers, we evaluated the relationship between the spectral power in 7 frequency bands and neural spike rates (Tables S1 and S2). Of the markers we considered, the normalized total LFP power in the 20–30 Hz band (Fig. 2C) tracked most faithfully the neural spike rate (Fig. 2B) during unconsciousness with the broadest dynamic range (see Tables S1 and S2). During unconsciousness, the correlation between the time courses of the normalized total power in the 20–30 Hz band and the normalized neural spike rates was 0.882 [95% confidence interval (0.875, 0.889)], based on 11 recording sessions (Fig. 2D). The corresponding mean dynamic range was 1.87 [95% confidence interval (1.56, 2.18)]. We constructed the MOU so that its lower (higher) values correspond to higher (lower) levels of unconsciousness. The neurophysiological results reported by Bastos et al. suggest that this MOU will reflect a global brain state and hence, that our CLAD system will control a global brain state [see Fig. 1G in Ref. (7)].

## PK–PD model of propofol's MOU

To relate the infusion of propofol to the amount of propofol in the effect-site—brain sites of anesthetic action—we assumed a two-compartment PK model (Fig. 3A, upper panel). We assumed a four-parameter logistic equation to define the PD model in order to relate the MOU to the effect-site amount (Fig. 3A, lower panel). The equations for the PK and PD models are given in Materials and Methods section (see section "PK–PD model and related parameter estimation from a given anesthesia recording session") (Eqs. 1 and 3, respectively). We illustrate the behavior of this PK–PD system with a simulated example (Fig. 3B). The input, a constant propofol infusion, (Fig. 3B, upper panel, $u(t)$) induces an exponential rise in the effect-site amount followed by an exponential decline after the infusion is stopped (Fig. 3B, middle panel). To conduct closed-loop control, we estimate the parameters of the combined PK–PD model. The combined PK–PD nonlinear least squares model fits to experimental data—the MOU as a function of time in response to the propofol infusion rate—are shown in Figs. 3C (NHP-B) and 3D (NHP-A). The estimated effect-site amounts (Figs. 3C and D, middle panels, red curves) show the predicted inverse relations with respect to the MOU data (Figs. 3C and D, lower panels, black dots). The relative errors for the model fits in Fig. 3C and D, and the corresponding parameter estimates are reported in the section "PK–PD model and related parameter estimation from a given anesthesia recording session". These results demonstrate that we can estimate a specific PK–PD model for each animal.

## Formulation of an NHP CLAD system

Previous CLAD studies have used linear quadratic regulators (LQR) and proportional-integral-derivative (PID)-based control schemes (21, 28, 29). For our NHP CLAD system, we adopted a two degree of freedom LQI scheme to exploit, as noted above, its optimal tracking and robustness properties. The details of the construction are in the section "Controller design parameters for a given subject"). In the simulated and live experiments, we consider the control to be accurate if the CLAD system tracks the target trajectory with minimal error, where we quantify the control error using the standard metrics in the section "Materials and methods" (Eqs. 32–35).

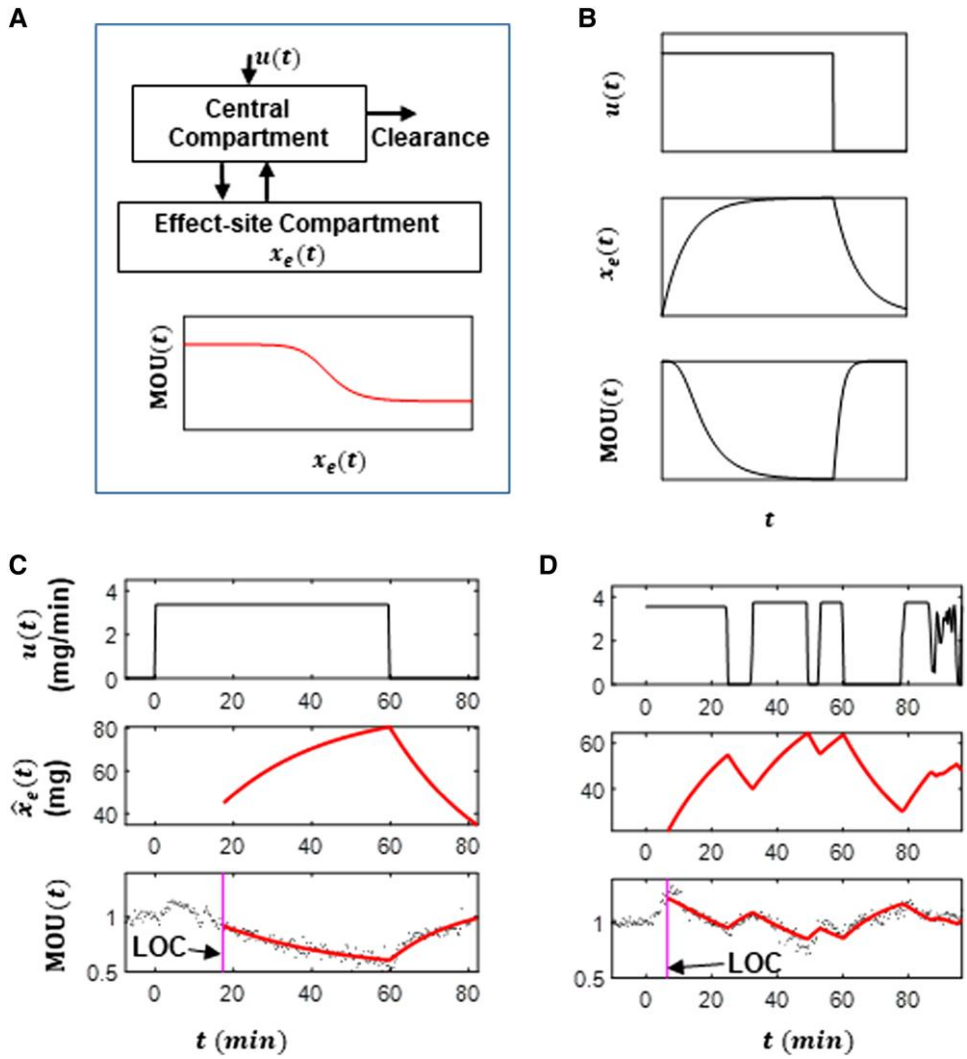


**Fig. 3.** PK and PD models for the CLAD system. A) (Upper figure) Two compartment PK model for propofol: $u(t)$ is the propofol infusion rate and $x_e(t)$ is the effect-site amount. (Lower figure) The PD model showing the assumed sigmoidal relation between the MOU and the effect-site amount. B) Simulation of PK–PD models for constant infusion rate of propofol $u(t)$ and the resultant effect-site amount $x_e(t)$ and MOU($t$). C) and D) show the PK–PD model fits to propofol infusion and MOU data from one experimental session from NHP-B and NHP-A, respectively. Top subpanel is the propofol infusion. Middle subpanel is the estimated time course of the effect-site amount. Lower panel is the observed MOU (black dots) and the MOU estimated (red curve) from the PK–PD model. LOC (vertical magenta line): loss of consciousness.

## CLAD system controls MOU in simulated experiments

We first tested our CLAD system in two simulated control experiments. We constrained the range of the propofol infusion rate to [0.0, 0.4] mg/kg/min, added Gaussian white noise to the PK–PD model output, and maintained constant infusion rates between each 20-s controller update. The assumed animal weight was 11 kg. Each simulated control experiment was divided into four stages and lasted 155 min (Fig. 4). During the first 30 min (stage 1), the system ran in an open-loop mode by maintaining a constant propofol infusion rate of 0.285 mg/kg/min (3.1 mg/min). During the remaining 125 min, the CLAD system controlled the propofol infusion rate: for the first 45 min to maintain the MOU at 1.05 (stage 2); for the second 40 min to maintain the MOU at 0.95 (stage 3); and for the final 40 min at 1.05 again (stage 4). We termed this inverted top-hat target profile Target Plan 1. In the first simulated experiment (Fig. 4A) we treated the PK–PD parameters as known by setting them to be same as those in the estimated PK–PD model used to develop the LQI controller (Fig. 4A). The CLAD system tracked the target trajectories well with median (25th and 75th percentiles) values of inaccuracy, bias, wobble, and divergence of 1.35% (1.34%, 1.67%), −0.14% (−0.71%, 0.04%), −0.017% (−0.019%, −0.005%), and 1.40%/min (1.31%/min, 1.62%/min), respectively, across the three target MOU levels. We next simulated a model misspecification scenario with Target Plan 1 in which the PK–PD parameters were higher by 20% than those used in the controller design. Despite misspecification, the target tracking was stable (Fig. 4B). The time to target convergence and the performance metrics [inaccuracy = 1.55% (1.43%, 1.60%), bias = −0.16% (−0.97%, − 0.00%), divergence = −0.019% (−0.024%, − 0.007%), wobble = 1.35%/min (1.32%/min, 1.52%/min)] agreed closely with those in the known parameter case (Fig. 4A).

## CLAD system controls MOU in live experiments

For the first live propofol CLAD experiments, we tested Target Plan 1 in three sessions in NHP-A (Fig. 5A–C). Performance across the three sessions was nearly identical. During the initial 30 min of open-loop control, propofol was maintained at a constant infusion rate of

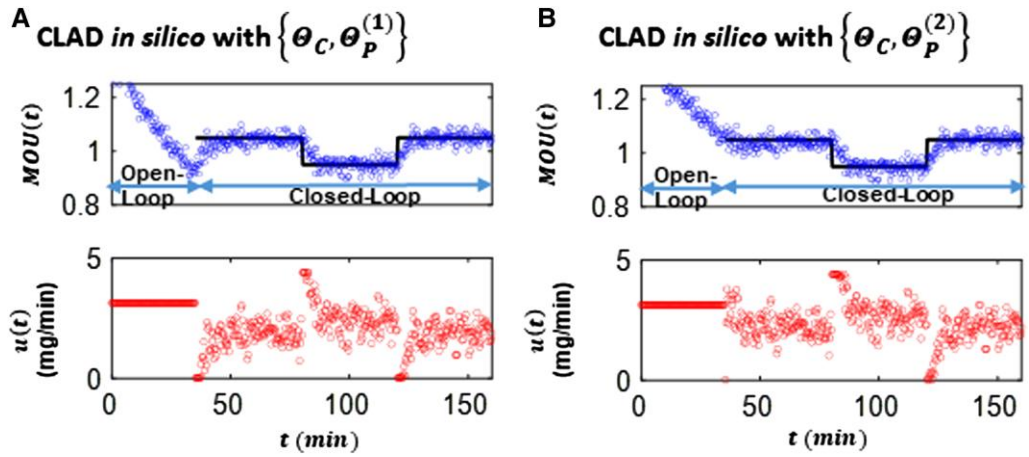


**Fig. 4.** Simulated CLAD experiments. Simulated CLAD Experiments using Target Plan 1 (see text in section "CLAD system controls MOU in simulated experiments"). Upper subpanel: Black line is the target trajectory. Blue dots are the CLAD system trajectory. Lower subpanel: Red dots are the propofol infusion rates determined by the CLAD system. A) The CLAD system control is executed with the PK–PD parameter set $\Theta_P^{(1)}$ and control parameter set $\Theta_C$ used in the system design. B) The CLAD system control is executed with PK–PD parameter set $\Theta_P^{(2)}$ not used in the system design.

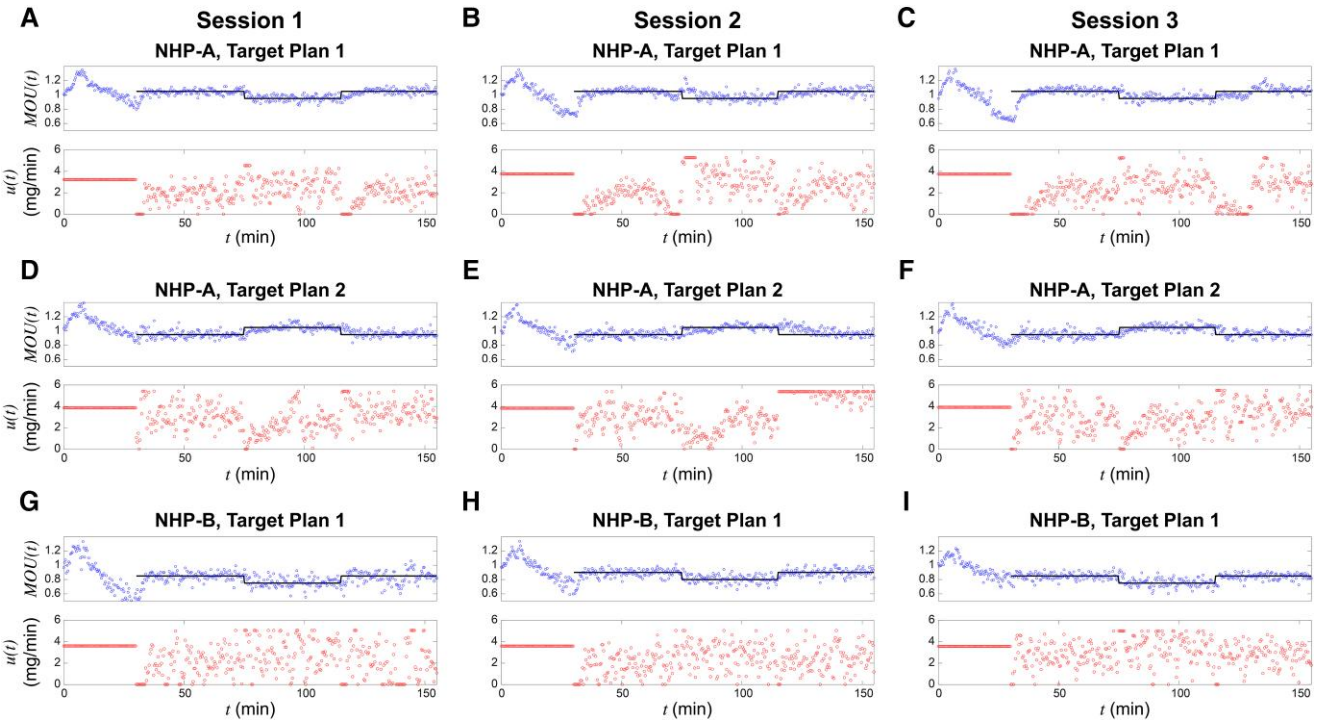


**Fig. 5.** *Live* CLAD experiments. *Live* CLAD experiments using Target Plans 1 and 2 (see text in section "CLAD system controls MOU in live experiments"). Upper subpanel: Black lines are the target trajectory. Blue dots are the MOU trajectory. Lower subpanel: Red dots are the propofol infusion rates determined by the CLAD system. A–C) Three CLAD experimental sessions with NHP-A using Target Plan 1. D–F) Three CLAD experimental sessions with NHP-A using Target Plan 2. G–I) Three CLAD experimental sessions with NHP-B using Target Plan 1.

0.285 mg/kg/min (3.7 mg/min) (Fig. 5A–C, lower panel, red dots). The MOU initially increased then decreased monotonically indicating that the NHP became more unconscious (Fig. 5A–C, upper panel, blue dots). At 30 min, the CLAD system took over the propofol infusion to initiate the first 45 min of closed-loop control. As in the simulation experiment, to increase the MOU level to 1.05 (Fig. 5A–C, upper panel, black line)—decreasing the level of unconsciousness—the CLAD system stopped the infusion for approximately 3 min (Fig. 5A–C, lower panel, red dots). Once the target level of 1.05 was acquired, the infusion restarted, and the controller varied the propofol infusion rate to keep the MOU at the target level. During the second 40 min of closed-loop control, the target MOU was decreased to 0.95, meaning a deeper level of unconsciousness. The CLAD system achieved the new target within approximately 2–4 min (Fig. 5A–C, upper panel, blue dots). The controller varied the infusion rate to control the MOU (Fig. 5A–C, bottom panel, red dots). For the final 40 min of closed-loop control the target level was reset to 1.05 (Fig. 5A–C, upper panel, black line). The CLAD system again achieved the new target level by stopping the infusion for approximately 4 min (Fig. 5A–C, lower panel, red dots). Once the target level of 1.05 was achieved, the CLAD systems again changed the infusion rate to maintain MOU control at this target level.

We conducted three more live CLAD experiments in NHP-A with Target Plan 2 (Fig. 5D–F). It had a top-hat profile consisting of: 30 min of a constant infusion rate at 3.7 mg/min; 45 min of closed-loop control at MOU level 0.95; 40 min of closed-loop control at MOU level 1.05; and 40 min control at MOU level 0.95. As with Target Plan 1 for NHP-A, during the first 30 min of open-loop control with propofol administered at a constant infusion rate, the MOU initially increased then monotonically decreased indicating a deeper level of unconsciousness (Fig. 5D–F, upper panel, blue dots). The difference between the final MOU value at the end of the open-loop period and the MOU target for the first control period was less than for any of the three sessions of Target Plan 1. Therefore, the controller did not stop the propofol infusion (Fig. 5D–F, lower panel, red dots) to achieve the initial target MOU of 0.95 (Fig. 5D–F, upper panel, black line). Control was well maintained for the three target MOU values in each of the three sessions. Of note in session 2, the controller used the maximal rate of 5.2 mg/min (Fig. 5E, lower panel, red dots) nearly nonstop to maintain control for the second MOU target value of 0.95 (Fig. 5E, upper panel).

Finally, we executed in NHP-B a nearly identical protocol to the NHP-A Target Plan 1 (Fig. 5G–I). We adjusted the MOU target levels so that the upper MOU level was 0.9 and the lower level was 0.8 to maintain an appropriate state of unconsciousness for NHP-B. The controller's performance for the three sessions of Target Plan 1 executed with NHP-B (Fig. 5G–I) agreed closely with its performance for this target plan in NHP-A (Fig. 5A–C).

During all the studies, the animals were physiologically stable. We measured oxygen saturation and heart rate from the pulse oximeter during each experiment. The electrocardiogram and blood pressure were not recorded. Oxygen saturations stayed above 90% and the heart rates ranged from 120 to 160 beats per minute. The animals breathed room air spontaneously. No emergency interventions were required to maintain hemodynamics, oxygenation or ventilation. These physiological responses were in close agreement with those reported by Bastos et al. (7), where the animals received constant infusions of propofol.

## Performance analysis for live control experiments

The boxplot summaries of the performance metrics for the live experiments suggest highly accurate performance (Fig. 6A) of our CLAD system with no appreciable overall bias (Fig. 6B), no appreciable temporal bias (Fig. 6C), and no unusually large fluctuations or error variability (Fig. 6D). The groups in the boxplots and the CLAD performance metrics are defined in the legend of Fig. 6 and section "Analysis of CLAD performance." The group 3 boxplots showed slightly higher variability for the MDAPE (Fig. 6A), comparable to the MDPE (Fig. 6B) and the Wobble (Fig. 6D). With the exception of a slightly higher percentiles for group 3, the standard deviations of the propofol infusion rates (Fig. 6E) were also comparable. The differences between the boxplots reflect animal variation since the groups 1 and 2 boxplots show results from NHP-A, whereas the group 3 boxplots give the results from NHP-B. The overall performance of our CLAD system for these two animals in terms of these metrics is comparable to performances in earlier human and rodent propofol-based CLAD studies (25, 26, 28) (also, see Table S4).

# Discussion

We have demonstrated that a propofol CLAD system can accurately control in the NHP, rhesus macaque, level of unconsciousness for the maintenance period of general anesthesia. Our CLAD system accurately controlled unconsciousness for 18 h and 45 min in nine experiments by tracking two different 125-min dynamic target trajectories in two different animals (Fig. 5). We limited the duration of the maintenance periods to approximately 2 h as these were preliminary investigations designed to demonstrate the feasibility of closed-loop control in NHPs as a steppingstone to the development of human systems. Our system performance was comparable or superior to that reported in previous CLAD studies (Tables S3 and S4).

The inputs to our CLAD system are the user-prescribed MOU target value and the current MOU value computed by the state estimation algorithm (Fig. 1). Every 20 s, our CLAD system computes a new output, the update of the propofol infusion rate. The current MOU value is easy to compute in real-time using standard multitaper spectral estimation methods (5, 32, 33) applied to the LFP recorded from a prefrontal cortical electrode. We established that the normalized LFP power in the 20–30 Hz band strongly correlated with normalized spike rate, a marker of propofol-mediated unconsciousness (Fig. 2) characterized in our previous studies (7). As a safety measure, our CLAD system has a user-set maximum infusion rate.

We used an optimal LQI control strategy (31, 35, 36) to control the output response of a linear time-invariant dynamical system with an additive disturbance. We set the LQI parameters so that for control of the linearized PK–PD model, the CLAD system had high gain and phase margins and a fast-settling time. When controlling the response of a nonlinear PK–PD model our CLAD system showed stable target tracking with error levels at or below those reported in previous studies (Table S4). Our optimal LQI strategy offers the flexibility to tune the controller to achieve both reliable target tracking and disturbance rejection. We tuned our LQI controller by devising subject-specific instantiations of the PK and PD models that characterized how the MOU changed with propofol dose (Fig. 3C and D). We used nonlinear least squares to estimate animal-specific PK–PD model parameters from MOU and drug-infusion rate data.

We began each experimental session by running our CLAD system with a constant infusion rate and no feedback control to simulate common operating room usage of propofol infusion systems in the United States to control unconsciousness. Target controlled infusions (TCI) have not been approved by the US FDA. Instead of the MOU remaining at a constant level, in each session it increased and then monotonically decreased, indicating that unconsciousness became progressively more profound (Fig. 5A–I). This likely relates to the known biphasic response of the neurophysiological parameters to propofol (37). To achieve the target level of unconsciousness once the CLAD system took over MOU control, the controller set the infusion rate to 0 for 3–8 min. This is a clinically relevant observation because it shows how the common practice of using constant infusion rates can lead to overdosing. This observation is particularly relevant for elderly patients who at standard propofol infusion rates readily drift into burst suppression, a profound level of unconsciousness associated with postoperative cognitive disorders (2, 12).

To date, most CLAD studies have maintained the control variable at a specific value for the duration of the study (19, 21, 23–25, 38, 39). In contrast, we maintained control of the MOU at a fixed value for 35–40 min then switched to control level of unconsciousness to another target MOU value (Fig. 5A–I). Therefore, we maintained a more refined control of unconsciousness. Such refined control is key at all times during surgery but especially for timing emergence from general anesthesia when it is important

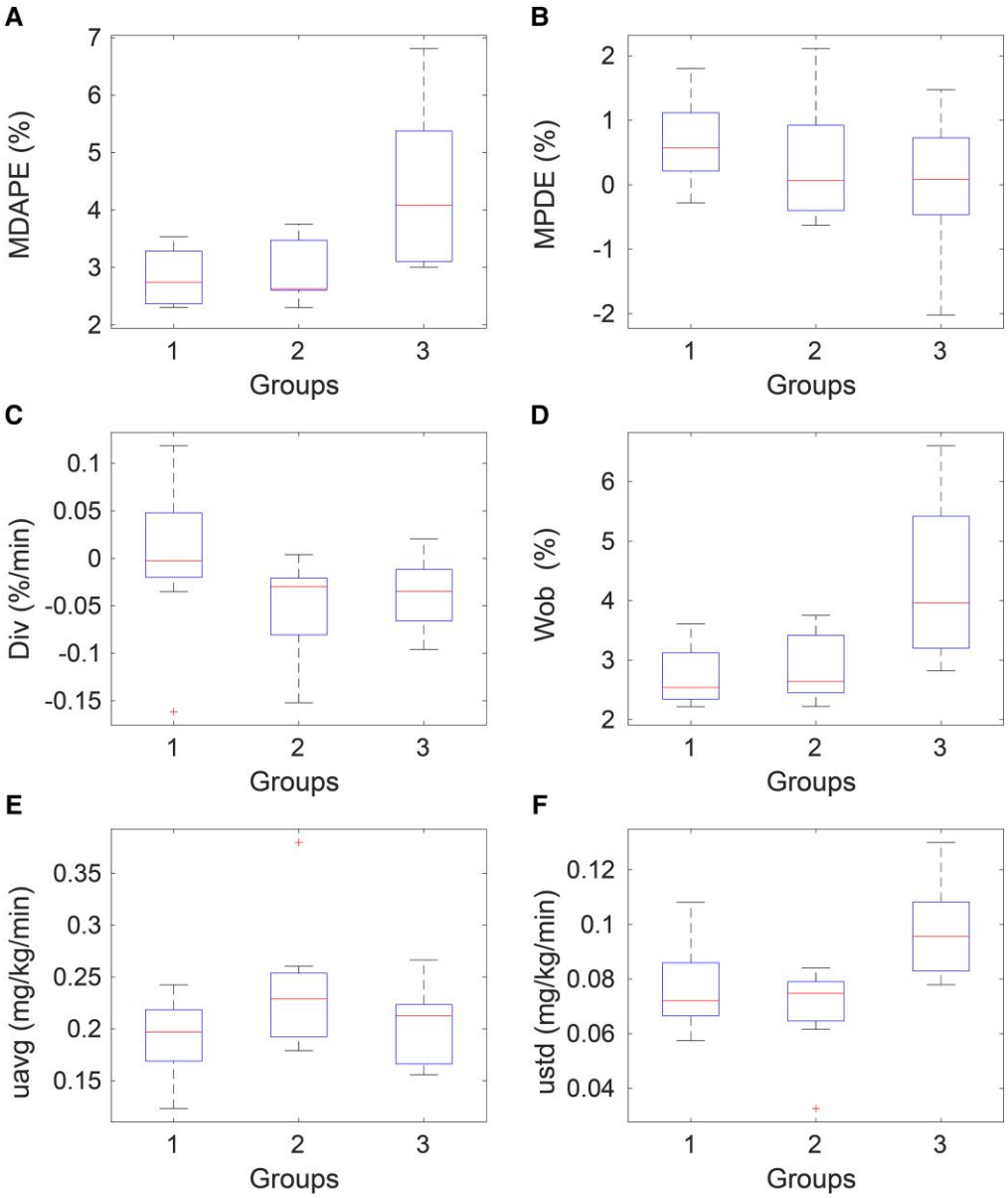


**Fig. 6.** Box plots of performance measures for the two NHPs and the two target plans. Groups 1–3, respectively, correspond to the three experimental designs: NHP-A with Target Plan 1, NHP-A with Target Plan 2, and NHP-B with Target Plan 1. A) Median absolute performance error (MDAPE). B) Median performance error (MDPE). C) Divergence (Div). D) Wobble (Wob). E) Average infusion rate (uavg). F) Standard deviation of the infusion rates (ustd).

to coordinate control over return of consciousness, movement, and spontaneous ventilation.

At present, computer-assisted administration of intravenous anesthetics is achieved using TCI systems in which the infusion rate is guided by population PK and PD models, and a user-specified target effect-site concentration to be achieved at a specific time (40, 41). Our CLAD system offers three important advantages over TCI systems. First, our system adapts the PK model to the individual subject by estimating subject-specific parameters. Second, the TCI system offers no way of knowing if the target effect-site is achieved. Third, the EEG is frequently used with TCI systems. However, it is not a component of this system. Therefore, because the TCI system lacks a PD model and feedback control, it cannot adjust the anesthetic infusion rate in real time based on a neurophysiological response of the patient to the anesthetic. Our CLAD system offers a principled way to combine PK and PD modeling and neurophysiological measurements to guide automated maintenance of unconsciousness.

Our CLAD system offers several key innovations. The first is successful use of a CLAD system to control unconsciousness in an NHP model. Our application in rhesus macaques demonstrates successful CLAD testing in an animal system whose central nervous (7, 42, 43), cardiovascular (44), renal (45), and hepatic systems (46) are established models for their human counterparts. By conducting our CLAD development with NHPs, we have followed the FDA's recommendation of using an animal model that is clinically, physiologically and anatomically relevant to humans (30). Second, we linked the LFP markers used in the CLAD system to sparse neuronal spiking activity, a clear neurophysiological correlate of unconsciousness characterized in our recent studies (7). Establishing this relationship was key for delineating the neurophysiological mechanisms underlying our MOU

and for constructing accurate PD models. Third, our CLAD system efficiently combined modern control theory principles and state estimation algorithms with parsimonious PK models and neurophysiologically validated PD models. Finally, our experimental and analytic paradigms can help guide critical pathways for soliciting FDA approval of CLAD systems for human testing (30).

In future research, we will develop a MOU based on scalp EEG recordings in our NHP model because in any eventual human studies, the MOUs will be computed in real-time from EEG measurements. In our next set of NHP studies, we will refine the definition of unconsciousness by correlating our EEG-based MOU with both neurophysiological and behavioral measures of unconsciousness (5, 47, 48). The propofol-induced dynamics in the 20–30 Hz LFP band in the NHPs resemble the dynamics observed in the alpha (8–12 Hz) and in the beta (13–24 Hz) ranges of the frontal EEG signals recorded from healthy, young human adults (5). The MOU in the humans will likely be based on the EEG power in these ranges and in the slow-delta (0.1–1 Hz) range. These are reliable markers of unconsciousness in humans for propofol and other GABAergic anesthetics (5, 49). Our current analyses assumed that the PD and PK model parameters were static. This assumption will likely not be valid as the time interval for control increases. Therefore, we will pursue adaptive parameter estimation as part of adaptive control strategies to further improve CLAD performance. The current instantiation of our CLAD system is designed to control maintenance of unconsciousness. Further work will be required to make it appropriate for control of induction and emergence. As stated above, the key transition to developinng the human CLAD system from the current work is identifying EEG markers of unconsciousness. Once identified, we will reinvestigate our choice of control strategies (50) using the EEG markers in simulated and eventually in live human experiments. The latter will require FDA approval. We are highly optimistic that the CLAD framework we have established for the NHP model can be successfully extended to humans.

# Materials and methods

## Experimental subjects and vascular access

All procedures followed the guidelines of the MIT Animal Care and Use Committee and the US National Institutes of Health. Two rhesus macaques (*Macaca mulatta*) aged 14 years (NHP-A, male, approximately 13 kg) and 16 years (NHP-B, male, approximately 14 kg) participated in these experiments. To receive its intravenous propofol infusion, each animal was acutely implanted with a 24 gauge catheter in an ear vein after administration of lidocaine to the overlying skin. The catheter was removed at the end of the session and reinserted at the start of the next session.

## Neural recordings

For neural recordings, both NHP-A and NHP-B had two chronically implanted $8 \times 8$ iridium-oxide contact microelectrode arrays (Utah arrays, Multiport: 1.0 shank length, 400 $\mu$m spacing, Blackrock Microsystems, Salt Lake City, UT) for a total of 128 electrodes per animal. The arrays in NHP-A are located in supplemental eye field (SEF) and the ventrolateral prefrontal cortex (vlPFC). The arrays in NHP-B are located in the dorsal lateral prefrontal cortex and the vlPFC. A common subdural site was used to ground and reference the PFC and SEF recordings.

LFPs were recorded at 30 kHz, low-pass filtered online with a cutoff of 250 Hz and downsampled to 1 kHz. Spiking activity was recorded by bandpass filtering the 30 kHz signal from 250 to 5 kHz, and manually thresholding. Blackrock Cereplex E headstages were used for digital recording through 2–3 synchronized Blackrock Cerebus Digital Acquisition systems.

## Experimental sessions

To conduct the experiments, the animals were head-fixed in a sitting posture using an implanted titanium head-post and placed in a noise-isolation chamber with white noise masking. During the CLAD sessions, the 1 kHz neural signal was made accessible within Matlab (The Mathworks, Inc, Natick, MA) workspace through the Blackrock *cbmex* interface. In both animals, LFP recordings from a preselected single PFC electrode were used for CLAD algorithm design and experimental testing. The single electrode was selected based on the observation by an NHP electrophysiology expert of multiunit activity characterized by distinct spike wave forms prior to experimental testing of the CLAD algorithm. From each subject, both raw signal at 30 KHz and a filtered 1 KHz signal low-passed below 250 Hz were recorded.

Infrared monitoring tracked facial movements, and pupil size (Eyelink 1000Plus, SR-Research, Ontario, CA) throughout the course of the experiments. Physiological monitoring of heart rate and oxygen saturation was performed by dedicated NHP anesthesia experts throughout the period of the recording to ensure safety of the animal (using Model 7500, Nonin Medical, Inc., Plymouth, MN). Occasionally, when oxygen saturation approached 90%, breathing support was provided manually using an ambu bag. Throughout each experiment session, we ensured that the oxygen saturation stayed steadily above 90% and subject was breathing spontaneously without intubation.

We conducted nine CLAD sessions divided as six for NHP-A and three for NHP-B. Each CLAD session consisted of two parts. In the first part, propofol was infused at a prespecified rate (open-loop control) of 0.285 mg/kg/min held after an initial baseline neural recording phase of at least 5 min. In the second part, and continuing from the first part without pause, we conducted closed-loop control of the MOU which we took to be the baseline normalized power in the 20–30 Hz band. During both parts of each session, propofol was infused intravenously using a computer-controlled syringe pump (PHD ULTRA 4400, Harvard Apparatus, Holliston, MA). We set the maximum allowable flow rate to 0.4 mg/kg/min in our computer program.

Prior to conducting the aforementioned 9 CLAD sessions in NHP-A and NHP-B, we used simultaneous neural activity and propofol infusion rate information from 11 additional recording sessions (10 of these from NHP-A) to determine the MOU. Of these 11 sessions, the chronologically last of the 10 sessions in NHP-A and the 1 session from NHP-B were used for PK–PD model fitting and NHP-specific control design.

## Spectral analysis of single-channel LFP from a given recording session

In both offline and online (real-time) spectral analysis of 1 KHz single-channel LFPs, we used nonoverlapping, consecutive data windows of $\Delta = 20$ s. We estimated the instantaneous power spectra using the multitaper spectral methods [Chronux Toolbox (51)] with the time-halfbandwidth product = 4 and number of tapers = 3. To calculate MOU for a given $\Delta$ interval, we computed first the LFP power (in dB) in 20–30 Hz range from the

corresponding multitaper spectrum. Then, the MOU estimate was determined by dividing this LFP power in 20–30 Hz band by a normalization factor. The normalization factor was the median of power from the same band determined from a 5-min period of data immediately prior to start of intravenous propofol infusion. In the offline setting, a smoothed estimate was obtained by fitting a cubic smoothing spline to the entire MOU sequence using Matlab function *csaps()* with its smoothing parameter set as $1/(1+\Delta^3/0.06)$. This smoothed estimate was used for both visualizing the MOU and estimating the session-specific PK–PD model parameters.

## Spike rate calculation from a given recording session

The spike rates were calculated offline by postprocessing the 30 KHz data from multiple channels in the same microelectrode array from which we selected the single electrode for MOU calculation (see section "Spectral analysis of single-channel LFP from a given recording session"). First, we band-passed the signal from each electrode between 250 and 5,000 Hz using a second-order Butterworth filter. Then we determined the standard deviation of 1-min segments of the signal from the middle of the anesthesia session. We used a threshold-based approach to detect multiunit activity where we identified all voltage activity whose magnitude exceeded 4.5× the estimated standard deviation. Then we explicitly imposed a 1.5-ms refractory period to identify a binary time-series of inferred spiking activity (such that 1 would indicate a single spike event, and 0 otherwise). From such binary time-series from significant spiking electrodes (whose total spike counts across the entire session exceeded 90th percentile from all channels in the relevant microelectrode array), we calculate the ensemble spike rate in the $k$th $\Delta$ interval by summing up all the 1's across all the channels from that interval and converting them to dB scale. Finally, to obtain the baseline normalized spike rate we divide spike rate sequence by the median value from the 5-min interval immediately prior to start of propofol infusion. For visualization purposes only, and similar to the approach used for the LFP MOU data (see section "Spectral analysis of single-channel LFP from a given recording session"), we estimate a smoothed spike rate sequence using Matlab function *csaps()* with its smoothing parameter set as $1/(1+\Delta^3/0.06)$.

## PK–PD model and related parameter estimation from a given anesthesia recording session

We define the PK component of the PK–PD model by the following continuous-time state-space equation (in modal form),

$$\frac{dx(t)}{dt} = Ax(t) + Bu(t), \tag{1}$$

where $x(t) = [x_1(t), x_2(t)]^T$ represents the propofol amount in a two-compartment mamillary PK model. Superscript $[\cdot]^T$ denoting a matrix transpose operation, $A$ is a diagonal matrix with $A_{1,1} = \lambda_1$ and $A_{2,2} = \lambda_2$ with $\lambda_2 < \lambda_1 < 0$, $B = [1, 1]^T$ is the input scaling matrix, and $u(t)$ denotes the infusion rate input (52). The inequality on the eigenvalues follows from the distinct, real-valued and nonpositive nature of eigenvalues of mamillary compartmental models (53). The amount of drug in the effect compartment is given by,

$$x_e(t) = [1, -1]x. \tag{2}$$

The sigmoidal function describing the decreasing trend in the MOU, $y(t)$, with increasing $x_e(t)$ during the period of unconsciousness is posited to be,

$$y(t) = \beta_0 - \beta_{\max}\frac{(x_e(t)/\beta_{50})^{\beta_c}}{1+(x_e(t)/\beta_{50})^{\beta_c}}, \tag{3}$$

where $\beta_0$, $\beta_{\max}$, $\beta_{50}$, and $\beta_c$ are positive scalar-valued parameters. To be precise, for a two-compartment mamillary model (Fig. 3A, top panel) $x_e \propto [1, -1]x$ (54), but we set it as an equality since the proportionality factor cannot be distinguished from $\beta$ when we seek to estimate all the PK–PD model parameters directly from $u(t)$ and $y(t)$ data [see Ref. (52, Sec. C) for details]. Therefore, the parameter set $\Theta_P = \{\beta_0, \beta_{\max}, \beta_c, \beta_{50}, \lambda_1, \lambda_2\}$ characterizes a PK–PD model.

To estimate $\Theta_P$ from a given recording session of duration $K\Delta$, we fit the PK–PD model to the available information on MOU $y_{1:K} \equiv \{y(k\Delta)\}_{k=1}^K$ at every $\Delta$ time interval and infusion rate history up to the same duration, $\{u(t): 0 < t < K\Delta\}$. To minimize the effect of the outliers in the optimization problem, we fit the model to a smoothed estimate of MOU $\{y_k^{(sm)}\}_{k=1}^K$ derived from $y_{1:K}$ (see section "Spectral analysis of single-channel LFP from a given recording session" for details on the smoothing operation). First, we set $\beta_0$ to be the maximum value that the MOU attains before starting its descent during a monotonically nondecreasing infusion rate of propofol. To estimate the other PK–PD parameters, we minimize the following objective function,

$$F(\Theta_P) = \sum_{k=L}^{H}\left(\beta_0 - \beta_{\max}\frac{(x_e(t)/\beta_{50})^{\beta_c}}{1+(x_e(t)/\beta_{50})^{\beta_c}} - y_k^{(sm)}\right)^2. \tag{4}$$

The time interval $[L\Delta, H\Delta]$ corresponded to the period of unconsciousness. By our choice of $L$ and $H$, note that our PK–PD model will be valid in our anesthetic regime of interest where the LFP marker decreases with increase in $x_e$. Starting with an initial guess, we estimate the parameters using an alternating optimization approach where we alternate between the two minimization problems to estimate the PD and PK parameters separately [similar in principle to our earlier work (52)].

The initial guesses for the PD parameters are given by $\beta_{\max}^{(0)} = 2\beta_0 - 2\min[\{y_k^{(sm)}\}_{k=1}^K]$, $\beta_{50}^{(0)} = \max[\{x_{e,k}^{(0)}\}_{k=L}^H]$, $\beta_c^{(0)} = 1$, where superscript $(\cdot)^{(0)}$ denotes the 0th iteration of the alternating optimization. The initial guesses for the PK parameters, $\lambda_1^{(0)}$ and $\lambda_2^{(0)}$, are set as the maximum and minimum eigenvalues of the transition matrix characterizing the PK of a two-compartment mamillary model for propofol PK in Japanese macaques derived as follows: In the absence of a propofol PK model for rhesus macaques, we consider a three-compartment linear model for propofol PK in Japanese macaques (55). We then derived a reduced order [a two-compartment mamillary model (54)] that has an impulse response function for the effect compartment most similar to the impulse response function for the central compartment of the three-compartment mamillary PK model (55).

In the $i$th iteration of the iterative alternating optimization approach, we first solve the following constrained optimization problem using Matlab's *fmincon()* function,

$$\{\beta_{\max}^{(i)}, \beta_c^{(i)}, \beta_{50}^{(i)}\} = \arg\min_{\beta_{\max}, \beta_c, \beta_{50}} F([\beta_{\max}, \beta_c, \beta_{50}, \lambda_1^{(i-1)}, \lambda_2^{(i-1)}]) \tag{5}$$

such that $\beta_{\max}^{(0)}/2 \le \beta_{\max} \le 5\beta_{\max}^{(0)}$, $\widehat{x}_{e,L}^{(0)} \le \beta_{50} \le 100\max[\{\widehat{x}_{e,k}^{(0)}\}_{k=L}^H]$, $0.1 \le \beta_c \le 20$ and,

$$\widehat{x}_{e,k}^{(i)} = \int_0^{k\Delta}(e^{(k\Delta-\tau)\lambda_1^{(i)}} - e^{(k\Delta-\tau)\lambda_2^{(i)}})u(\tau)\,d\tau. \tag{6}$$

After solving the optimization problem in Eq. 5, we solve another optimization problem

$$\{\lambda_1^{(i)}, \lambda_2^{(i)}\} = \underset{\lambda_1, \lambda_2}{arg\,min}\ F(\{\beta_{max}^{(i)}, \beta_c^{(i)}, \beta_{50}^{(i)}, \lambda_1, \lambda_2\}) \quad (7)$$

such that $-10,000 < \lambda_1 < \lambda_2 < 0$. We alternate between the two optimization problems, Eqs. 5 and 7, for a prescribed maximum number of iterations (50 iterations in our implementations). Finally, we determine the inaccuracy between the estimated MOU $\hat{y}$ and the given data y using a relative error metric calculated as $100 \times (\sum_{k=L}^{H} (\hat{y}_k - y_k^{(sm)})^2)^{1/2} / (\sum_{k=L}^{H} (y_k^{(sm)})^2)^{1/2}$. The relative error metric for the model fits in Fig. 3A and B were 5.94% and 5.13%, respectively. The parameter estimates $(\hat{\beta}_{(max)}, \hat{\beta}_{50}, \hat{\beta}_c, \hat{\lambda}_1, \hat{\lambda}_2)$, corresponding to Fig. 3A and B, were (5.6826, 327.1569, 1.6261, −0.0377, −509.4326) and (5.2299, 249.8976, 1.7543, −0.0425, −509.4326), respectively.

## Controller design parameters for a given subject

In choosing our control strategy, we considered existing strategies reported in literature that can enable the output of the system being controlled (the MOU response in the current case) to track a user-prescribed target value (target MOU). Those strategies were favored that were similar to ones that have precedence in the CLAD literature, such as the optimal control framework [linear quadratic regulator (LQR) strategy with estimated state feedback] for CLAD as in our prior rodent studies (28, 29) and the proportional-integral-derivative (PID) control framework for CLAD as used in human subjects outside the United States (25, 39, 56). In a separate simulation-based study, we verified that a hybrid approach based on a linear quadratic itegral (LQI) control, with the principled optimization-based design framework of LQR control and the stable output tracking property under model uncertainty of a proportional-integral (PI) control, could stably control the PD response of propofol PK–PD models of human subjects (57). This inspired us to choose the LQI scheme that updates the infusion rate by combining two components: an LQR strategy and an integral compensation strategy that monitors accumulation of the tracking error ($MOU_{target} - MOU_{actual}$) (31, 35, 36). The LQR component uses an observer to estimate the propofol effect-site level (31, 58). Since LQR, when coupled to an estimator, can be sensitive to model mis-specification, the inclusion of an integral compensation can ensure stable MOU tracking even when the PK–PD model is mis-specified. Hence, the integral compensation helps ensure a degree of robustness in our control strategy. In addition to the aforementioned benefits, the chosen LQI control framework (originally proposed by Hagiwara et al. (31, 35, 36) for a general linear time-invariant system with step targets and disturbances) provides a principled optimization-based framework to design a two-degree-of-freedom controller for a linear system with step targets and step disturbances. The "two-degree-of-freedom" feature of the controller stems from the fact that the response to step targets and to step disturbances can be tuned separately without affecting the performance of either. For the LQI control this is done by minimizing two distinct quadratic criteria. The solution of the first leads to the LQR feedback gains and the solution to the latter characterizes the integral action and observer gains. The control design is characterized by the set of user-prescribed parameters that goes in the definitions of the quadratic criteria.

Choosing the LQI strategy was just the first step towards our CLAD controller design (see Fig. S3A for an overview and Fig. S4 for detailed block diagram of the same LQI strategy). Tuning the parameters of the controller such that the CLAD has desired properties was the next step. Since the optimal LQI control strategy was developed for linear systems, we linearized a PK–PD model (estimated from each NHP) about a steady-state infusion rate of $u_{SS} = 0.285$ mg/kg/min, a value that we determined empirically to be a safe dose for maintaining unconsciousness during a prolonged experimental session for the NHP. The steady-state values for the PK state, $x_{SS}$ and for the MOU, $y_{SS}$ were calculated as follows. According to the PK model (Eqs. 1 and 2) the steady-state values for the PK states is given by

$$x_{ss} = -A^{-1}Bu_{ss}, \quad (8)$$

$$x_{e,ss} = [1, -1]x_{ss}. \quad (9)$$

Then steady-state response $y_{SS}$ is calculated by substituting $x_e$ with $x_{e,ss}$ in Eq. 3. Assuming that the CLAD operation will be primarily in the neighborhood of this steady state, the next step was to derive the following linear systems approximation that captured the dynamics in the deviation of the state and MOU about the steady state.

$$\frac{d\tilde{x}}{dt} = A\tilde{x} + B\tilde{u}, \quad (10)$$

$$\tilde{y} \approx C_{u_{ss}}\tilde{x}, \quad (11)$$

where $\tilde{y} = y - y_{ss}$, $\tilde{x} = x - x_{ss}$, $\tilde{u} = u - u_{ss}$, and $C_{u_{ss}} = (dy/dx_e)_{x_e = x_{e,ss}}[1, -1]$.

From this step onwards, the feedback control problem was rephrased as that of output tracking problem (where $\tilde{y}$ should track a constant target value, $\tilde{y}_{tar} \equiv y_{tar} - y_{ss}$) of a linear time-invariant system with additive disturbance terms, $d_x$ and $d_y$.

$$\frac{d\tilde{x}}{dt} = A\tilde{x} + B\tilde{u} + d_x, \quad (12)$$

$$\tilde{y} = C_{u_{ss}}\tilde{x} + d_y. \quad (13)$$

This formulation of the feedback control problem with system dynamics given by Eqs. 12 and 13 was amenable to controller design per Hagiwara et al.'s two-degree-of-freedom LQI control framework (31, 35, 36). The optimal feedback control, $\tilde{u}_c$, is calculated as

$$\tilde{u}_c = u_1 + u_2 + u_3, \quad (14)$$

where $u_1$ is an output of an LQR control block, $u_2$ is a feedforward value that would account for nonzero setpoint, $\tilde{y}_{tar}$, and $u_3$ corresponds to the control contribution due to integral compensation (see Fig. S4 for detailed block diagram). The LQR control, $u_1$ in Eq. 14, is given by

$$u_1 = K_C\hat{\tilde{x}}, \quad (15)$$

where $K_C$ denotes the LQR gain and $\hat{\tilde{x}}$ denotes the estimated deviation of the state from its nominal value $x_{ss}$. Here, the LQR gain, $K_C$, can be calculated as

$$K_C = -R^{-1}B^TX_1, \quad (16)$$

where $X_1$ represents the solution of the following algebraic equation,

$$A^TX_1 + AX_1 - X_1BB^TX_1 + Q = 0, \quad (17)$$

where $Q$ and $R$ are user-prescribed parameters to enforce a design choice specifying contributions of deviations in state trajectory and deviation in control trajectory, respectively, to

a quadratic criterion that is minimized (28, 36, 59). We further impose structure on the parameters Q and R as follows:

$$Q = \begin{bmatrix} \frac{\alpha_1}{(x_{1,\max} - x_{1,ss})^2} & 0 \\ 0 & \frac{\alpha_2}{(x_{2,\max} - x_{2,ss})^2} \end{bmatrix}, \quad (18)$$

$$R = \frac{\rho}{(u_{\max} - u_{ss})^2}, \quad (19)$$

where $x_{1,\max}$ and $x_{2,\max}$ are steady-state values corresponding to a user-prescribed $u_{\max}$ (= 0.4 mg/kg/min in this work). Therefore, LQR design is characterized by $\alpha_1$, $\alpha_2$, and $\rho$. The dynamics of the estimate $\widehat{\tilde{x}}$ is governed by the following differential equation:

$$\frac{d\widehat{\tilde{x}}}{dt} = \widehat{A}\widehat{\tilde{x}} + B\tilde{u}_c - K_E\tilde{y}, \quad (20)$$

where $\widehat{A} = A + K_E C_{u_{ss}}$ (58). A stable estimator design can be specified by choosing the estimator gain, $K_E$, such that $\widehat{A}$ has negative eigenvalues. Following Hagiwara et al. (31), in this work, $K_E$, is prescribed as a Kalman Filter-like gain, per,

$$K_E = -W_y^{-1} C_{u_{ss}} X_2, \quad (21)$$

where $X_2$ represents the solution of the following equation:

$$AX_2 + A^T X_2 - X_2 C_{u_{ss}}^T C_{u_{ss}} X_2 + W_x = 0. \quad (22)$$

Again, $W_x$ and $W_y$ are design parameters that can be regarded as terms that capture the variability in the process dynamics and the measurements, respectively [similar in principle to covariance matrices of random noise terms in the process and observation equation of a Kalman Filter (60)]. Following Hagiwara et al. (31), we impose the following structure on $W_x$ and $W_y$:

$$W_x = \sigma^2 BB^T, \quad (23)$$

$$W_y = 1. \quad (24)$$

Therefore, specifying σ enforces a design choice for the estimator dynamics. Furthermore, the feed-forward input $u_2$ in Eq. 14 is given by

$$u_2 = H_0 \tilde{u}_{tar}, \quad (25)$$

where the feed-forward gain, $H_0$ is given by

$$H_0 = -(C_{u_{ss}}(A + BK_C)^{-1}B)^{-1}. \quad (26)$$

In the absence of disturbances and modeling errors, the term $u_3 = 0$ in Eq. 14 is zero (36). When disturbances and modeling errors are present, $u_3$ acts as a correction term enabling output tracking via an integral compensation. The expression for $u_3$ in Eq. 14 is given by

$$u_3 = G\left(\Gamma\widehat{\tilde{x}} + \int_0^t (y_{tar} - y(t'))\, dt'\right), \quad (27)$$

where $\Gamma \equiv C_{u_{ss}}(A + BK_C)^{-1}$. Note that $u_3$ has contributions from both the estimator output and the integral of the output tracking error. Following Hagiwara et al. (36), the gain $G$ is given by

$$G = -\kappa^{-1}(-H_0^{-1})^T X_3. \quad (28)$$

In the above Eq. 28, $X_3$ satisfies the following equation:

$$-X_3(-H_0^{-1})\kappa^{-1}(-H_0^{-1})^T X_3 + \xi = 0, \quad (29)$$

where κ and $\xi$ are user-prescribed positive-valued scalar design parameters that enforce design choices on disturbance rejection properties of the controller when disturbances and model misspecifications are present.[1] Similar to the Q and R, the terms $\xi$ and κ serve to enforce design choices for disturbance rejection properties in another quadratic criterion that is minimized to determine G per Eq. 28 (36). In the current implementation, we set $\kappa = 1$, and prescribe $\xi$ as a design parameter. Therefore, the linear controller design for a given NHP is specified by the set of parameters, $\Theta_C = \{\Theta_P, \alpha_1, \alpha_2, \rho, \sigma, \xi\}$, where $\Theta_P$ represents the set of PK–PD parameters from a given NHP used to design the respective CLAD algorithm.

By using the continuous-time framework of the LQI control strategy, one can determine the loop transfer function and consequently determine metrics that capture the robustness of the controller and convergence dynamics. This information can be determined by using the *margin()* and *stepinfo()* subroutines from Matlab's Control System Toolbox with the loop transfer function as an argument. The loop transfer function can be calculated as a product of two complex-valued functions $G_P(s)$ and $G_Y(s)$, where

$$G_P(s) = C_{u_{ss}}(sI - A)^{-1}B, \quad (30)$$

$$G_Y(s) = -(1 - (G\Gamma + K_C)(sI - \widehat{A})^{-1}B)^{-1}\left(-\frac{G}{s} - (G\Gamma + K_C)(sI - \widehat{A})^{-1}K_E\right) \quad (31)$$

and $s$ denotes a complex number.

In simulation studies (as shown in Fig. 4), we tested the ability of this linear feedback control strategy to provide acceptable tracking performance when the dose-effect-site relationship was governed by the NHP's PK–PD model. To mimic actual experimental conditions in our simulations, we imposed the lower and upper limits ($u_{min} = 0$ mg/kg/min and $u_{\max} = 0.4$ mg/kg/min) on the suggested control $u_c$ to determine the actual control signal $u$ that is communicated to the infusion pump. Furthermore, we added to the PK–PD model output a Gaussian white noise with zero mean and standard deviation of 0.02. The standard deviation value was empirically determined from the residual error between observed MOU and the estimated MOU using the best fitting PK–PD model. We enforced fixed rate of infusion between each discrete controller updates. This simulation strategy is illustrated in Fig. S3B. For a given NHP's PK–PD model, $\Theta_P$, we tuned the free parameters, $\{\alpha_1, \alpha_2, \rho, \sigma, \xi\}$ and tested each candidate controller design in *in silico* experiments that comprised a 125 closed-loop simulation with 3-step input changes at 0, 45, 85 min after a 30-min open-loop simulation under constant infusion rate of 0.285 mg/kg/min. Through this manual tuning exercise, we selected an NHP-specific control design $\Theta_C$ (with $\alpha_1 = 10^6$, $\alpha_2 = 1$, $\rho = 10^4$, $\sigma = 10^{-3}$, $\xi = 10^4$, and $\Theta_P$ set to parameter estimates for NHP-A (or, NHP-B) as reported in section "PK–PD model and related parameter estimation from a given anesthesia recording session") such that the open-loop transfer function ($-G_P G_Y$) had high phase margin (>80°), high gain margin (>60 dB) and low settling times for a unit step input (<11 min), and the CLAD performance was acceptable in simulation experiments. The performance criteria chosen was that of inaccuracy being less than 5% across the 125 min of closed-loop simulation. Briefly, a high gain margin for the control design indicates that the closed-loop system will still remain stable even when the true system has a multiplicative gain factor that was unaccounted during control design. The margin provides the extent to which this unaccounted gain factor can be tolerated. Similarly, a high phase margin would indicate that the closed-loop system would still remain stable even when the

[1] Even in an ideal case when the true PK–PD parameters are available the model used in the control design can still be misspecified due to unaccounted nonlinearities (present in the true model) during the linearization step.

true system has delay (up to an extent specified by the margin) that was unaccounted during control design. Lower settling times for a unit step indicates faster convergence of MOU to target when a new target value is encountered. High gain, high phase margins, and low settling times are desirable properties for a CLAD design.

### Analysis of CLAD performance

The controller performance was analyzed using the sequence of data $\{(y_k, u_k)\}$ where $y_k$ and $u_k$, respectively, denoted the MOU value and the infusion rate at the time-point $t_k$ (say, prescribed in minutes), where $k \in \{1, \ldots, K\}$ with $k = 1$ and $k = K$ denoting the beginning and the end of a temporal segment. Using this data and the definition of instantaneous performance error, $e_k = 100(y_k - y_{tar})/y_{tar}$, several CLAD performance metrics that are typically used in literature can be calculated (28, 39, 61, 62). The metrics that we analyze are: median absolute performance error (MDAPE), median performance error (MDPE), wobble (Wob), and divergence (Div). These are defined as follows:

$$\text{Inaccuracy, MDAPE}\,(\%) = \text{median}[\{|e_k|,\ k = 1, \ldots, K\}], \tag{32}$$

$$\text{Bias, MDPE}\,(\%) = \text{median}\big[\{e_k,\ k = 1, \ldots, K\}\big], \tag{33}$$

$$\text{Wobble, Wob}\,(\%) = \text{median}\big[\{|e_k - \text{MDPE}|,\ k = 1, \ldots, K\}\big], \tag{34}$$

$$\text{Divergence, Div}\,(\%/\text{min}) = \frac{\sum_{k=1}^{K} |e_k| t_k - \left(\sum_{k=1}^{K} |e_k|\right)(1/K)\left(\sum_{k=1}^{K} t_k\right)}{\sum_{k=1}^{K} t_k^2 - (1/K)\left(\sum_{k=1}^{K} t_k\right)^2}. \tag{35}$$

The MDAPE is a measure of the inaccuracy in CLAD performance for the entire analysis period. The MDPE is a measure of the bias in the MOU target tracking, with a positive (or, a negative) value indicating that the MOU lies mostly above (or, below) the target value. Wobble is a measure of the intra-session time-related variability, with a high wobble value indicating a higher degree of oscillation of the controlled MOU about its target. Divergence characterizes any linear trend in the performance error over time, with a positive value suggesting that the MOU is gradually diverging away from the target, whereas a negative value suggesting a gradual converging of the MOU towards the target. Additionally, we also report the average (denoted by $u_{avg}$) and dispersion (as measured by standard deviation and denoted by $u_{std}$) of the infusion rates across the $K$ data-points.

## Acknowledgments

The authors acknowledge the help provided by Dr. Robert Marini, Dr. Alexis Garcia, Dr. Jefferson Roy, Dr. Scott Brincat, Dr. Jesus Ballesteros, Jordan DeFarias, and Anna Rock with animal surgery and animal care, and/or operational details towards experiments, data curation, and data analysis. S.C. thanks Dr. Jingzhi An, Dr. John Abel, Dr. Gabriel Schamberg, Dr. Dimitrios Papageorgiou, Devika Kishnan, Ksenia Nikolaeva, David Zhou, and John Tauber, for helpful discussions and for initial code snippets. S.C. further thanks Dr. Francisco Flores, Dr. Christa Van Dort, Dr. Yumiko Ishizawa, and Dr. Michelle McCarthy for additional helpful discussions.

## Supplementary material

Supplementary material is available at *PNAS Nexus* online.

## Funding

This research was supported by the JPB Foundation; the Picower Institute for Learning and Memory; Bill and Cheryl Swanson, George J. Elbaum, Mimi Jensen, Diane B. Greene, Mendel Rosenblum, annual donors to the Anesthesia Research Initiative Fund; and the NIH Awards P01GM118269 (E.N.B., E.K.M. and S.C.), R01NS123120 (E.N.B. and E.K.M.) and R01MH115592 (E.K.M. and E.N.B.).

## Author contributions

E.N.B., S.C., and E.K.M. contributed to conceptualization. S.C. and A.S.W. contributed to data curation. S.C. and E.N.B. did formal analysis. E.N.B. and E.K.M. contributed to funding acquisition. S.C., J.D., A.S.W., and M.M. did investigation of the study. S.C., J.D., and M.M. contributed to methodology. E.N.B. and E.K.M. contributed to resources. S.C., A.S.W., and I.C.G. contributed to software. E.N.B. and E.K.M. did supervision of the study. S.C. did validation of the study. S.C. contributed to visualization. Writing—original draft: S.C. and E.N.B. Writing—review editing: S.C., E.N.B., E.K.M., J.D., A.S.W., M.M., I.C.G., and S.G.

## Data availability

All the analyzed data used, custom scripts for data analysis, and data visualization are available at *PNAS Nexus* online.

## References

1 Brown EN, Lydic R, Schiff ND. 2010. General anesthesia, sleep, and coma. *N Engl J Med*. 363(27):2638–2650.
2 Brown EN, Pavone KJ, Naranjo M. 2018. Multimodal general anesthesia: theory and practice. *Anesth Analg*. 127(5):1246.
3 Epstein BS. 1987. ASA adopts standards for the practice of anesthesiology. *Arch Surg*. 122(10):1215–1216.
4 Lewis LD, *et al.* 2012. Rapid fragmentation of neuronal networks at the onset of propofol-induced unconsciousness. *Proc Natl Acad Sci USA*. 109(49):E3377–E3386.
5 Purdon PL, *et al.* 2013. Electroencephalogram signatures of loss and recovery of consciousness from propofol. *Proc Natl Acad Sci USA*. 110(12):E1142–E1151.
6 Purdon PL, Sampson A, Pavone KJ, Brown EN. 2015. Clinical electroencephalography for anesthesiologists part I: background and basic signatures. *Anesthesiology*. 123(4):937–960.
7 Bastos AM, *et al.* 2021. Neural effects of propofol-induced unconsciousness and its reversal using thalamic stimulation. *eLife*. 10: e60824.
8 Garwood IC, *et al.* 2021. A hidden Markov model reliably characterizes ketamine-induced spectral dynamics in macaque local field potentials and human electroencephalograms. *PLoS Comput Biol*. 17(8):1–28.
9 Rohan D, *et al.* 2005. Increased incidence of postoperative cognitive dysfunction 24 h after minor surgery in the elderly. *Can J Anaesth*. 52(2):137–142.
10 Robinson TN, Eiseman B. 2008. Postoperative delirium in the elderly: diagnosis and management. *Clin Interv Aging*. 3(2):351–5.
11 Krenk L, Rasmussen LS. 2011. Postoperative delirium and postoperative cognitive dysfunction in the elderly—what are the differences? *Minerva Anestesiol*. 77(7):742–749.
12 Evered L, *et al.* 2018. Recommendations for the nomenclature of cognitive change associated with anaesthesia and surgery-2018. *Anesthesiology*. 129(5):872–879.

13 Gaskell A, Sleigh J. 2021. The quagmire of postoperative delirium: does dose matter? *Br J Anaesth*. 127(5):664–666.
14 Swarbrick CJ, L Partridge JS. 2022. Evidence-based strategies to reduce the incidence of postoperative delirium: a narrative review. *Anaesthesia*. 77(S1):92–101.
15 Evered LA, *et al.* 2021. Anaesthetic depth and delirium after major surgery: a randomised clinical trial. *Br J Anaesth*. 127(5):704–712.
16 Gibbs FA, Gibbs EL, Lennox WG. 1937. Effect on the electroencephalogram of certain drugs which influence nervous activity. *Arch Intern Med*. 60(1):154–166.
17 Bickford RG. 1950. Automatic electroencephalographic control of general anesthesia. *Electroencephalogr Clin Neurophysiol*. 2(1–4): 93–96.
18 Kiersey DK, Bickford RG, Faulconer A Jr. 1951. Electro-encephalographic patterns produced by thiopental sodium during surgical operations; description and classification. *Br J Anaesth*. 23(3):141–52.
19 Schwilden H, Stoeckel H, Schüttler J. 1989. Closed-loop feedback control of propofol anaesthesia by quantitative eeg analysis in humans. *Br J Anaesth*. 62(3):290–296.
20 Absalom AR, Sutcliffe N, Kenny GN. 2002. Closed-loop control of anesthesia using bispectral indexperformance assessment in patients undergoing major orthopedic surgery under combined general and regional anesthesia. *Anesthesiology*. 96(1):67–73.
21 West N, *et al.* 2013. Robust closed-loop control of induction and maintenance of propofol anesthesia in children. *Paediatr Anaesth*. 23(8):712–719.
22 West N. 2018. Design and evaluation of a closed-loop anesthesia system with robust control and safety system. *Anesth Analg*. 127(4):883–894.
23 Liu N. 2006. Titration of propofol for anesthetic induction and maintenance guided by the bispectral index: closed-loop versus manual control: a prospective, randomized, multicenter study. *Anesthesiology*. 104(4):686–695.
24 Liu N, *et al.* 2011. Closed-loop coadministration of propofol and remifentanil guided by bispectral index: a randomized multicenter study. *Anesth Analg*. 112(3):546–557.
25 Puri GD, *et al.* 2016. A multicenter evaluation of a closed-loop anesthesia delivery system: a randomized controlled trial. *Anesth Analg*. 122(1):106–114.
26 Struys MM, *et al.* 2001. Comparison of closed-loop controlled administration of propofol using bispectral index as the controlled variable versus "standard practice" controlled administration. *Anesthesiology*. 95(1):6–17.
27 Vijn PC, Sneyd JR. 1998. IV anaesthesia and EEG burst suppression in rats: bolus injections and closed-loop infusions. *Br J Anaesth*. 81(3):415–421.
28 Shanechi MM, Chemali JJ, Liberman M, Solt K, Brown EN. 2013. A brain–machine interface for control of medically-induced coma. *PLoS Comput Biol*. 9(10):e1003284.
29 Ching S, *et al.* 2013. Real-time closed-loop control in a rodent model of medically induced coma using burst suppression. *Anesthesiology*. 119(4):848–860.
30 Parvinian B, Scully C, Wiyor H, Kumar A, Weininger S. 2018. Regulatory considerations for physiological closed-loop controlled medical devices used for automated critical care: Food and Drug Administration workshop discussion topics. *Anesth Analg*. 126(6):1916.
31 Hagiwara T, Furutani E, Araki M. 1997. Optimal observers for disturbance rejection in two-degree-of-freedom LQI servo systems. *IEE Proc, Control Theory Appl*. 144(6):575–581.
32 Babadi B, Brown EN. 2014. A review of multitaper spectral analysis. *IEEE Trans Biomed Eng*. 61(5):1555–1564.
33 Mitra PP, Pesaran B. 1999. Analysis of dynamic brain imaging data. *Biophys J*. 76(2):691–708.
34 Popilskis SJ, Kohn DF. 1997. Chapter 11—Anesthesia and analgesia in nonhuman primates. In: Kohn DF, Wixson SK, White WJ, John Benson G, editors. Anesthesia and analgesia in laboratory animals. San Diego (CA): Academic Press. p. 233–255.
35 Hagiwara T, Furutani E, Araki M. 1994. Two-degree-of-freedom design method of LQI servo systems: performance deterioration by the introduction of an observer and optimal observer design. In: Proceedings of 1994 33rd IEEE Conference on Decision and Control, Lake Buena Vista, FL, USA. IEEE. Vol. 4. p. 4204–4209.
36 Hagiwara T, Furutani E, Araki M. 1996. Two-degree-of-freedom design method of linear-quadratic servo systems with an integral compensator: analysis of the performance deterioration by the introduction of an observer. *Int J Control*. 64(5):941–958.
37 Schnider TW, *et al.* 1999. The influence of age on propofol pharmacodynamics. *Anesthesiology*. 90(6):1502–1516.
38 Liu N, *et al.* 2012. Feasibility of closed-loop titration of propofol and remifentanil guided by the spectral M-Entropy monitor. *Anesthesiology*. 116(2):286–295.
39 Dumont GA, Martinez A, Ansermino JM. 2009. Robust control of depth of anesthesia. *Int J Adapt Control Signal Process*. 23(5): 435–454.
40 Schnider TW, Minto CF, Struys MMRF, Absalom AR. 2016. The safety of target-controlled infusions. *Anesth Analg*. 122(1):79–85.
41 MRF Struys M, *et al.* 2016. The history of target-controlled infusion. *Anesth Analg*. 122(1):56–69.
42 Phillips KA, *et al.* 2014. Why primate models matter. *Am J Primatol*. 76(9):801–827.
43 Redinbaugh MJ, *et al.* 2020. Thalamus modulates consciousness via layer-specific control of cortex. *Neuron*. 106(1):66–75.e12.
44 Cox LA, *et al.* 2017. Nonhuman primates and translational research—cardiovascular disease. *ILAR J*. 58(2):235–250.
45 Timchalk C, Finco D, Quast J. 1997. Evaluation of renal function in rhesus monkeys and comparison to beagle dogs following oral administration of the organic acid triclopyr (3,5,6-trichloro-2-pyridinyloxyacetic acid). *Fundam Appl Toxicol*. 36:47–53.
46 Wang H, *et al.* 2015. Rhesus monkey model of liver disease reflecting clinical disease progression and hepatic gene expression analysis. *Sci Rep*. 5:15019.
47 Guay CS, *et al.* 2023. Breathe-squeeze: pharmacodynamics of a stimulus-free behavioural paradigm to track conscious states during sedation. *Br J Anaesth*. 130(5):557–566.
48 Ishizawa Y, *et al.* 2016. Dynamics of propofol-induced loss of consciousness across primate neocortex. *J Neurosci*. 36(29): 7718–7726.
49 Akeju O, *et al.* 2014. Effects of sevoflurane and propofol on frontal electroencephalogram power and coherence. *Anesthesiology*. 121(5):990–998.
50 Chakravarty S, Waite AS, Abel JH, Brown EN. 2020. A simulation-based comparative analysis of PID and LQG control for closed-loop anesthesia delivery. In: Proceedings of the IFAC World Congress, Berlin, Germany. Elsevier. Vol. 53. p. 15898–15903.
51 Bokil H, Andrews P, Kulkarni JE, Mehta S, Mitra PP. 2010. Chronux: a platform for analyzing neural signals. *J Neurosci Methods*. 192(1):146–151.
52 Chakravarty S, *et al.* 2017. Pharmacodynamic modeling of propofol-induced general anesthesia in young adults. In: 2017 IEEE Healthcare Innovations and Point of Care Technologies (HI-POCT), Bethesda, MD, USA. IEEE. p. 44–47.

53 Anderson DH. 2013. *Compartmental modeling and tracer kinetics*. Vol. 50. Berlin: Springer Science & Business Media.

54 Schwilden H. 1981. A general method for calculating the dosage scheme in linear pharmacokinetics. *Eur J Clin Pharmacol*. 20(5): 379–386.

55 Miyabe-Nishiwaki T, *et al.* 2013. Evaluation of the predictive performance of a pharmacokinetic model for propofol in Japanese macaques (*Macaca fuscata fuscata*). *J Vet Pharmacol Ther*. 36(2):169–173.

56 Dumont GA, Ansermino JM. 2013. Closed-loop control of anesthesia: a primer for anesthesiologists. *Anesth Analg*. 117(5):1130–1138.

57 Chakravarty S, Waite AS, Abel JH, Brown EN. 2020. A simulation-based comparative analysis of PID and LQG control for closed-loop anesthesia delivery. *IFAC-PapersOnLine*. 53(2):15898–15903. 21th IFAC World Congress.

58 Luenberger D. 1966. Observers for multivariable systems. *IEEE Trans Autom Control*. 11(2):190–197.

59 Aström KJ, Murray RM. 2010. *Feedback systems: an introduction for scientists and engineers*. Princeton (NJ): Princeton University Press.

60 Shumway RH, Stoffer DS. 2017. *Time series analysis and its applications: with R examples*. New York (NY): Springer Cham.

61 Varvel JR, Donoho DL, Shafer SL. 1992. Measuring the predictive performance of computer-controlled infusion pumps. *J Pharmacokinet Biopharm*. 20(1):63–94.

62 Struys MMRF, *et al.* 2004 Mar. Performance evaluation of two published closed-loop control systems using bispectral index monitoring: a simulation study. *Anesthesiology*. 100(3): 640–647.